Swirl mixing at microfluidic junctions due to low frequency side channel fluidic perturbations

Adrian Neild [a,*], Tuck Wah Ng [a], Gregory J. Sheard [b], Matthew Powers [a], Stefano Oberti [a,c]

[a] Laboratory for Optics, Acoustics and Mechanics, Department of Mechanical & Aerospace Engineering, Monash University, VIC 3800, Australia
[b] Fluids Laboratory for Aeronautical and Industrial Research (FLAIR), Department of Mechanical and Aerospace Engineering, Monash University, VIC 3800, Australia
[c] Center of Mechanics, ETH Zurich, CH-8092 Zurich, Switzerland

ARTICLE INFO

ABSTRACT

Swirl mixing between the input arms of a microfluidic system using vibration (Lab Chip 9 (2009) 1435–1438 [20]) has been shown to provide rigorous blending within a very short length along the flow stream. Investigations here, both numerical and experimental, indicate that this is due to an asymmetry in the manner in which liquid enters and exits a channel into a confined space. Based on this understanding, we demonstrate an alternative approach that applies low frequency side channel fluidic perturbations. This approach permits versatility in having mixing occur selectively anywhere along the flow stream, isolates and ensures that mixing occurs only at these locations, as well as minimizes movement so that image blurring, which limits the ability to assess mixing effectiveness optically, is reduced.

1. Introduction

Microfluidic systems are now widely used in chemical and biochemical applications in which efficient mixing of two or more streams of fluids is highly sought after. The challenge of mixing at the microscale lies with the domination of viscous over inertia forces which engender laminar flows. Passive microfluidic mixers are simple and inexpensive to operate. They typically require the induction of complex flow schemes along the fluidic channel [1–3]. Active systems, alternatively, require external energy input for mixing and have been based on cross-stream architectures [4,5], bacterial chemotaxis [6], electrokinetic instabilities [7], and laser excitation [8]. The benchmark of a highly efficient mixer nevertheless lies not only on the ability to achieve rigorous blending, but also within a short length along the flow stream. In this respect, the use of mechanical perturbation appears to offer advantages.

While there is increasing interest in the use of vibration as an actuation method within microfluidic systems, most efforts are concerned with high frequency schemes. Acoustic radiation forces have been widely used to manipulate suspended particles in microfluidic channels [9,10] and chambers [11,12]. Typically frequencies in the high kHz/low MHz range are used to achieve this. As these forces arise due to non-linear terms in the Navier–Stokes equations which time average (over an oscillatory cycle) to non-zero values, a net (time independent) force can be established by

appropriate integration over the particle surface. These non-linear terms can also act directly on the fluid causing acoustic streaming which can be used to cause active mixing [13,14] or movement of droplets in open systems [15]. Typically high frequency waves are actuated via relatively complicated micromachined actuators [16,17]. Droplet movement up an inclined surface [18] and particle manipulation [19] have both been recently demonstrated using low frequency excitation which has an inherently far simpler actuator requirement involving mounting the system on a shaker.

A recent active mixing approach of using low frequency vibration for mixing has been demonstrated to introduce unexpected strong swirling flow patterns at the inlet T-junction of a microfluidic system [20]. This contrasts with the type of mixing obtained through axis-symmetrical flow conditions at inlet T-junctions [21]. It is well known that swirling engenders high degrees of mixing in macroscale systems [22]. It should be noted that mixing by mechanical perturbations has been rarely reported at low frequencies. A method that applies peristaltic flow variations has been demonstrated [23] and modelled [24] in which the flow passing through the two arms leading to the T-junction (when most effective) has an out-of-phase pulsing nature (of the type $A + B\cos(\omega t)$ in one arm and $A - B\cos(\omega t)$ in the other). The mechanism in which mixing ensues is ascribed to the increasing surface area between the two fluids as they meet. As the higher velocity fluid penetrates into the lower velocity fluid, it results in a finger formation that reverses in the direction of each cycle. A somewhat parallel approach has the perturbation delivered through multiple side channels present along the flow stream [4,5]. The essential idea is then to interrupt the flow to the extent that chaotic patterns appear in order to facil-
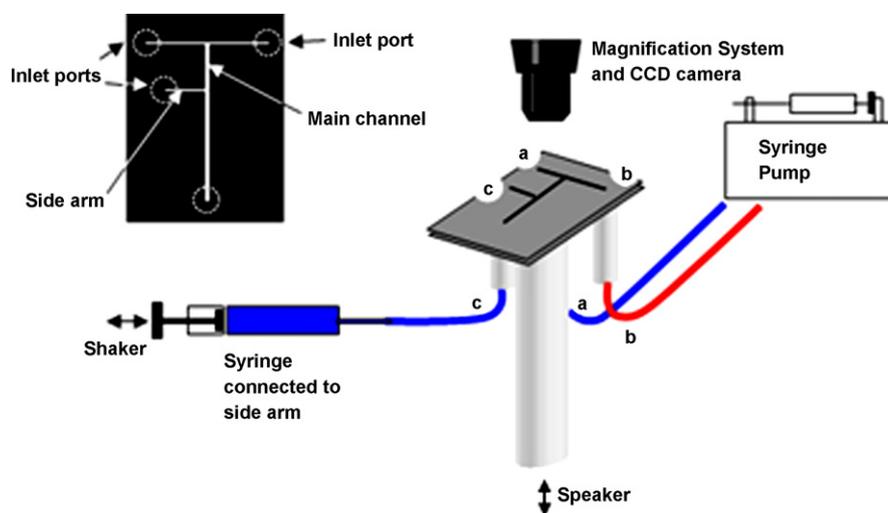
Fig. 1. A depiction of the micromachined fluidic channel, consisting of a main channel (formed at the junction of two smaller channels with inlets "a" and "b"), and of a side arm which forms a right angle junction with the main channel and is accessed via port "c". The experimental set-up required vibration to be induced, this was done in one of two ways. The first method was to use a speaker (driven by a signal generator) to vibrate the whole chip vertically. The second was to vibrate the fluid in the side arm, this used a shaker (driven by signal generator and amplifier) for activation. A syringe pump was used for controlled flow through the main channel and a magnification system and CCD camera for image capture.

itate mixing. A modification of this approach by changing the flow frequency and amplitude across the side channels has been shown to produce mixing that is attributed mainly to vortices that create multiple layers of liquid and Taylor–Aris dispersion [25].

In the prior demonstration of the vibration based method [20], the entire microfluidic system in which two liquids were incoming at a T-junction was vibrated predominantly in the orthogonal direction (to the plane of the chip). Here, we investigated, numerically and experimentally, the mechanics of the swirl mix phenomenon reported earlier [20] and reveal that it is predominantly driven by an asymmetric input and output of flow from side channels. This results in an ability to mix at the location of input of two incoming fluids when they first merge into a single stream. Using the understanding of the mechanism gained we offer, through a different set-up, the additional feature that mixing can be caused at defined location in the two fluid flow stream. In addition, this method will be ideal to be able to isolate and ensure that mixing occurs only at selected specific locations in the microfluidic system. An added advantageous feature will be a minimization in movement so that image blurring, which limits the ability to assess mixing effectiveness optically, is reduced.

2. Experimental and numerical method

The microfluidic channel used consists of two T-Junctions; firstly two channels measuring 250 μm in width joined to form a channel of 500 μm. At a distance of 5 mm from this junction a channel of width 250 μm (we will refer to this, henceforth, as the side arm) meets with the main 500 μm wide channel at 90° (forming the second T-junction). The structure has been dry etched into a 300 μm thick silicon wafer to a depth of 200 μm. Subsequently, this was sealed with a 500 μm thick glass wafer using anodic bonding. The reverse side of the silicon was etched such that open ports allowed fluidic connection with each channel end. A diagram is shown in Fig. 1. The fluid is pumped through the channels using a syringe pump (KD Scientific, model 200 series) with pipes connected to Luer-lok fittings on the reverse side.

In contrast to the previous approach of obtaining mixing at the fluid inlets [20], we focus on the ability to do so at the vicinity of a side channel of the microfluidic channel. Low frequency mechanical perturbation was achieved in two ways; via the entire system, and

thru a liquid column that feeds into the system. With the former, actuation is primarily in the vertical direction with a speaker that is driven by a signal generator (Stanford Research SDR 345). With the latter, actuation was done via pulsing a syringe attached to a shaker (LDS, model V201) excited by the same signal generator through a power amplifier (LDS, model PA25E).

Image recordings were made using a CCD camera (KP-D20AU, Hitachi) connected to a magnification lens (InfiniVar Video Microscope, Infinity Photo-Optical Company). The images were recorded at 25 frames per second directly onto a standard DVD recorder. Subsequently images obtained by playback from the DVD were transferred into a PC via a frame grabber driven by imaging software (Alliance Vision, Vision Stage).

Numerical simulations were computed using an incompressible Navier–Stokes solver employing a high-order spectral-element method for discretization in space and a third-order scheme for time integration [26,27]. A two-dimensional model of the second T-junction was produced which discretized the vicinity of the inter-
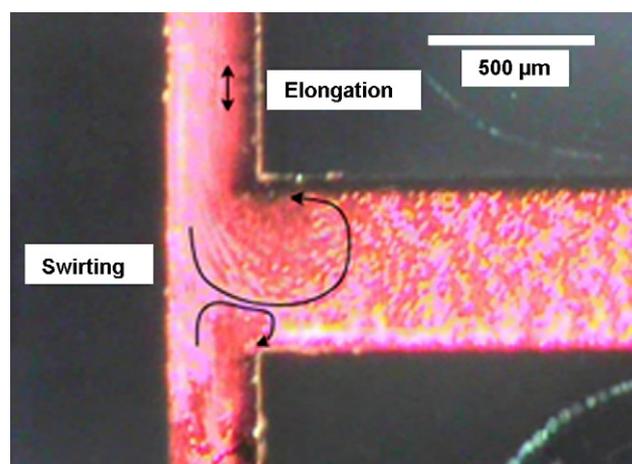
Fig. 2. An images showing the motion of suspended particles within a fluidic chip, when the whole chip is oscillated vertically (out of image plane). The shutter speed of the camera is slower than the vibrational frequency so the particles appear elongated (as labelled), the swirling effect (more clearly observed from video footage) has been indicated by arrows.
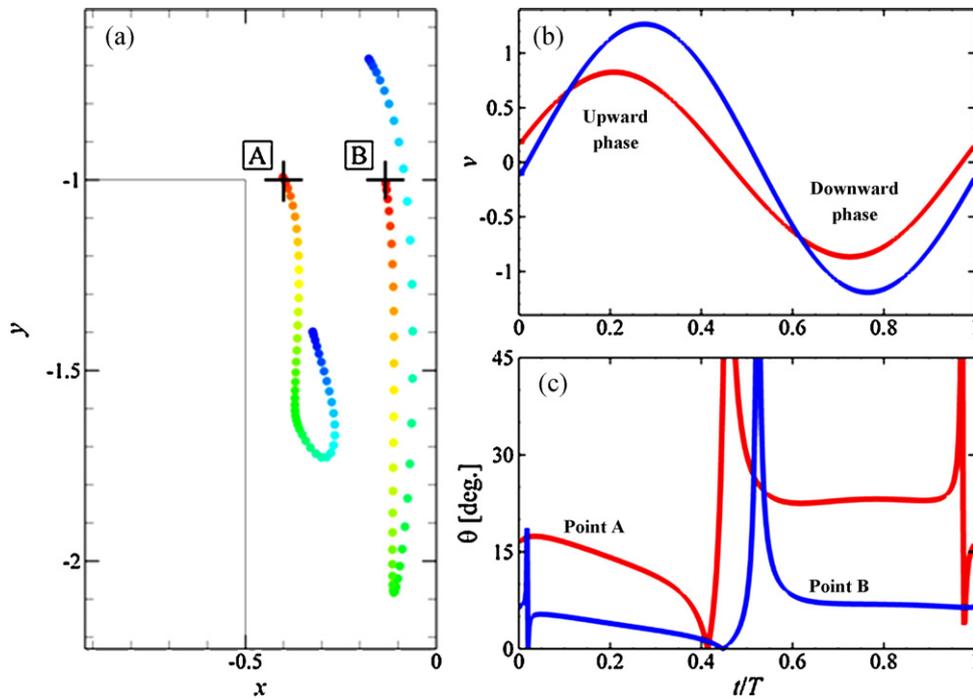
Fig. 3. (a) A plot of streaklines traced by particles injected from points on a line at the intersection of the main channel and side arm. The flow has been evolved over a single period, as shown in (b), and particles are coloured for their injection time, with blue the oldest and red the most recently injected. The centreline of the side arm is at $x = 0$, and lengths are normalized by the side-arm width (i.e. one unit length corresponds to 250 μm). (b) A plot of the component of velocity perpendicular to the main channel (v) over a single oscillation period at points A (red) and B (blue), where positive v is towards the main channel centreline from the side channel. (c) A plot of the magnitude of the angle of velocity from the perpendicular (θ) at points A and B. (For interpretation of the references to color in this figure legend, the reader is referred to the web version of the article.)

section of the main 500-μm wide channel and the side arm to high resolution, and also included 1250-μm lengths of channels extending in all directions from the junction. 137 elements with a polynomial degree of 6 were used to resolve the flow, and 500 time steps per oscillation period were employed to ensure that the simulations were accurate in time. No-slip boundary conditions were imposed on the velocity field on all channel walls, and time-varying Dirichlet velocity boundary conditions were used to impose a sinusoidal oscillation of fluid within the junction, driven from the 250-μm channel to replicate the laboratory conditions.

To study the mixing mechanism, simulation of the transport of passive tracer particles was conducted. The solver employed a scheme developed by Coppola et al. [28]. This scheme efficiently exploits the high spatial accuracy available with the spectral-element method, and this implementation has recently been validated [26,27].

3. Results

Firstly, we examine the fluid motion when the whole system is mounted horizontally and vibrated in the vertical direction. The fluidic network was filled with 15 μm diameter copolymer particles (Bangs Laboratories Inc.) which were suspended in water (with a concentration of approximately 5% solids) with a low pro-
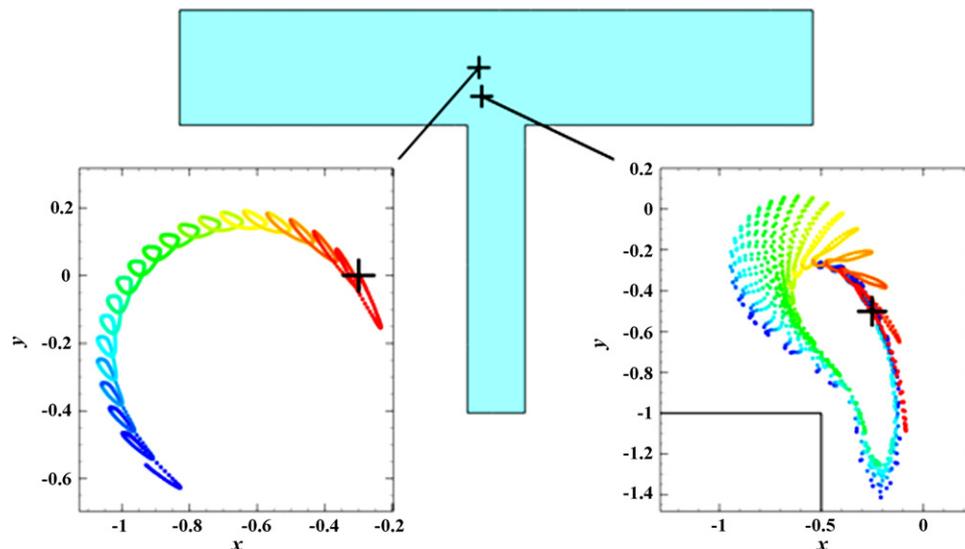
Fig. 4. Plots of streaklines traced by particles injected into the flow for 20 oscillation periods at points shown on the schematic of the second T-junction. Particle injection points are denoted by crosses, and as with Fig. 3, particles are coloured for their injection time, with blue the earliest and red the most recent.
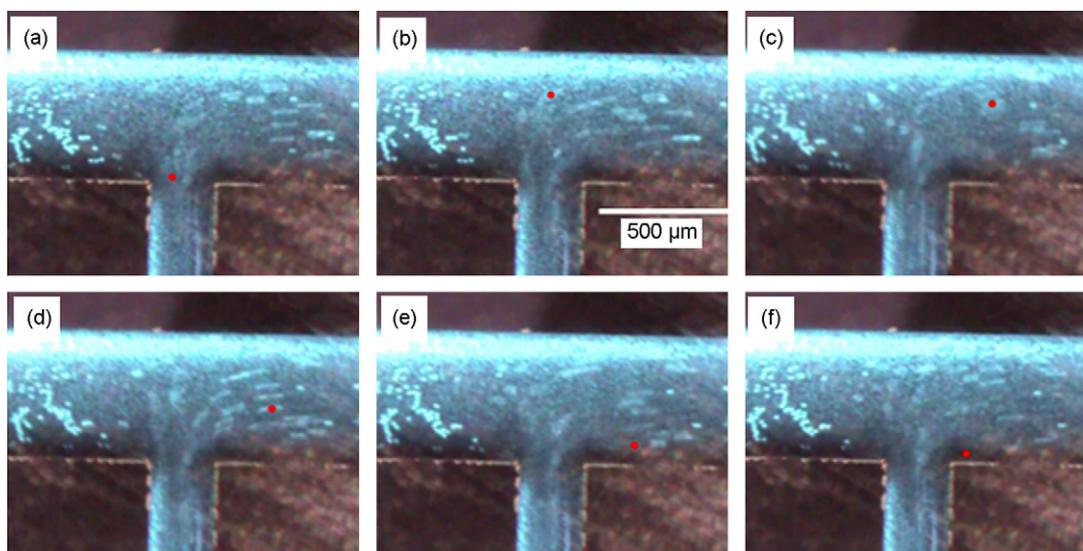
Fig. 5. A series of images occurring approximately 0.3 s apart, showing suspended particles swirling at the junction of the side arm and main channel. A red dot has been added for ease of tracing the pattern formed. It can be seen that the swirl on the right-hand side (in which the red dot is located) covers a larger area than the swirl on the left hand side. There is no net flow emerging from the side arm, and no flow pumped through the main channel. (For interpretation of the references to color in this figure legend, the reader is referred to the web version of the article.)
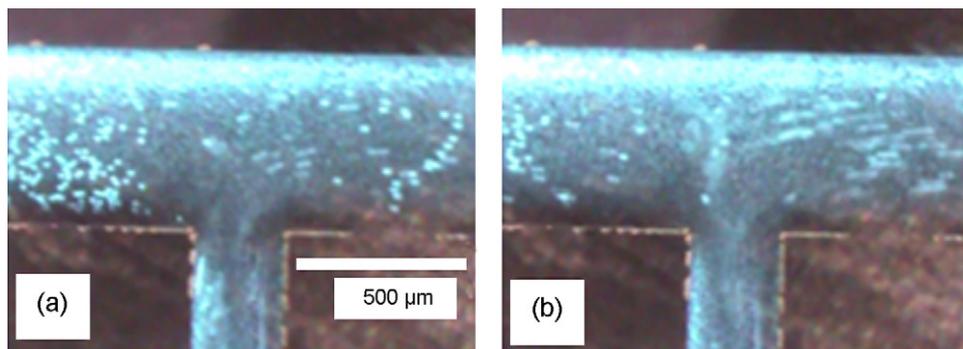
Fig. 6. Images using a shutter speed considerable longer than the period of oscillation of suspended particles moving due to side arm excitation of amplitude (a) 45 μm and (b) 60 μm. In the former vibration, observed as particle elongation occurs up to a distance of 260 μm away from the side arm exit, whilst for the later this distance increases to 550 μm.
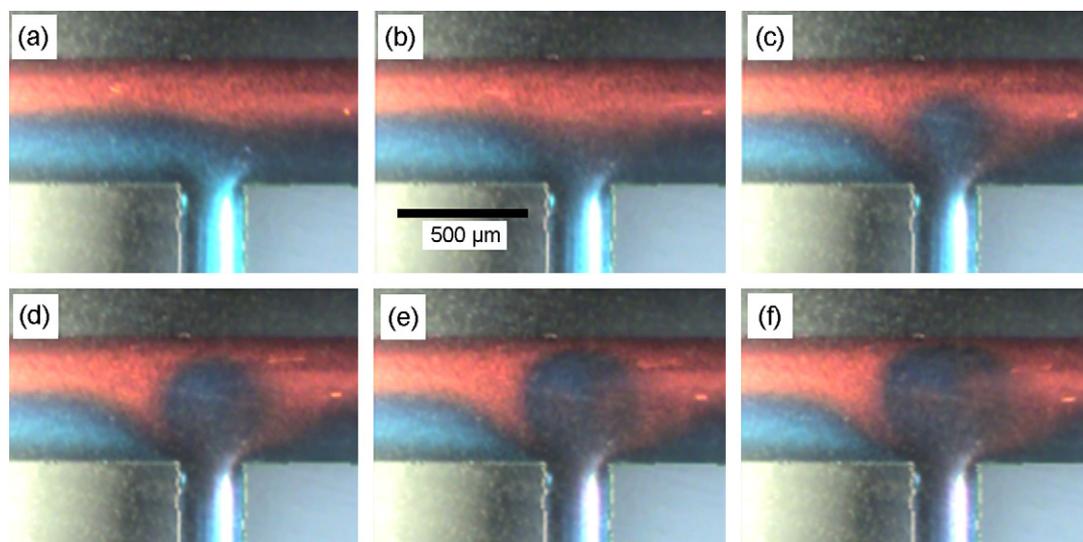
Fig. 7. This series of images, each separated by 0.04 s, shows the creation of a plume feature within the main channel at the point at which a junction is formed with the side arm. In this experiment red and blue dyed fluids have been introduced through the small channels feeding the main channel, and the side arm has been filled with blue fluid. There is no flow through the main channel and no net flow in the side arm. The fluid in the side arm has been excited via vibration at 100 Hz with a drive signal of a strength which produces a fluid oscillation amplitude 45 μm. The plume starts of blue (c), but as it grows more red fluid is drawn inside (d–f). (For interpretation of the references to color in this figure legend, the reader is referred to the web version of the article.)
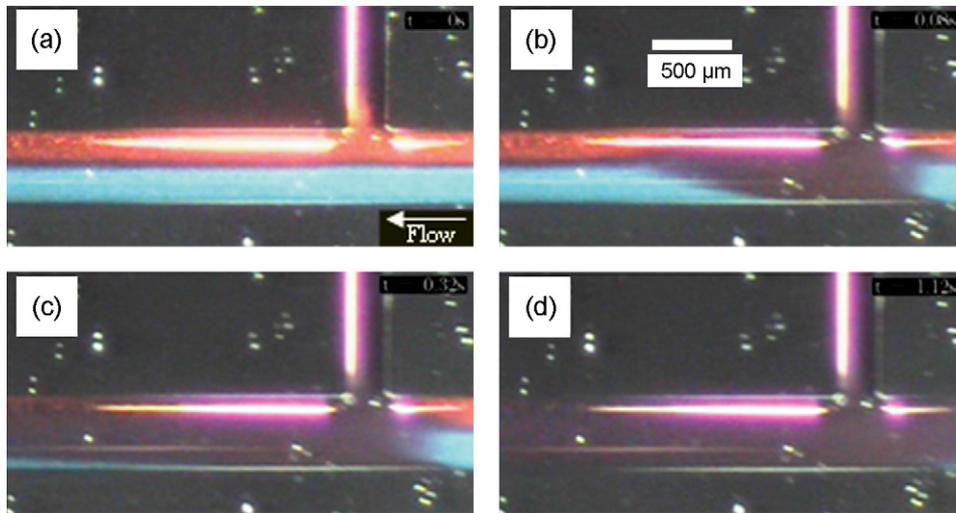
Fig. 8. These four images spanning a time of 1.12 s, show the evolution of a mixed fluid regime when the whole fluidic chip is vibrated in the direction normal to its plane. In (b) mixing starts to occur at the junction of the side arm and main channel, the mixed fluid is carried along the main channel (left ward) by the 0.01 ml/min flow in the main channel, this continues through (c). In (d) the portion of the channel rightward of the junction is also mixed in nature, this is not due to events taking place at the junction within view as fluid movement is leftward, instead it demonstrates than the junction at the entrance to the main channel (out of view on the right-hand side) also causes mixing. So the mixing can occur at any junction in the system, and as such is not well defined in its location.

portion (approximately 10% of the fluid) of red dye included to improve optical contrast. When excited at 100 Hz with no externally imposed flow, strong swirling patterns were visible as have been described previously [20]. Fig. 2 shows a still image of the particles during this process. The image has been annotated to show the swirling pattern. Of more immediate importance is the elongated appearance of the particles in the side channels. The vibration frequency is much higher than the frame rate, so we view the movement of the particle over a few full cycles. The elongation of the particle in the image demonstrates that there is an oscillation of the fluid in the side channels with an amplitude of approximately 60 μm (upper arm in the image), and this is a result of the vertical (out of image plane) excitation. In addition, the fluid is static prior to activation in this experiment, hence mixing is obtainable even when there is no net flow through the junction. Upon activation, the fluid in the input side channels pulse backwards and forwards.

These observations lead us to suspect that an asymmetry in the manner in which liquid entered and left the input channels was responsible for the swirling. On the forward part of the cycle, the fluid emerged from the channel into the more open space provided by the junction in the form of a jet; characterised by the highest localised flow rate being in the direction parallel to the channel from which the jet emerged. In the reverse part of the cycle, the fluid is drawn into the channel, in which it does almost equally from all directions. When done sufficiently fast, this will result in swirling at the point of intersection. This behaviour has similarity to the circulating flows described by Dijkink et al. in the context of a bubble vibrating at resonance in a short capillary for propulsion [29].

Numerical simulations were employed to isolate the mixing mechanism identified in this study. Key to this mechanism is the demonstration of symmetry-breaking in the oscillating flow
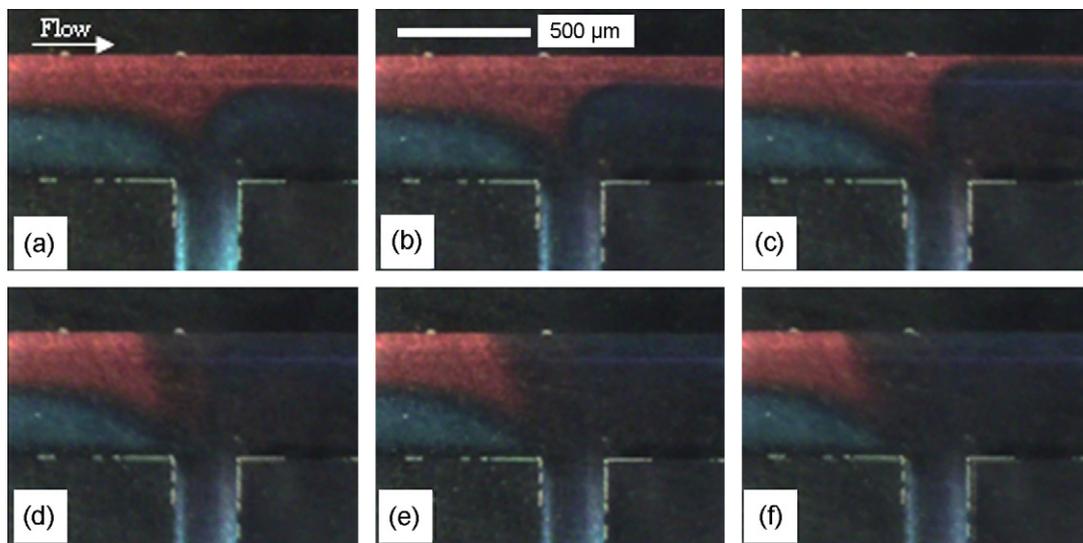
Fig. 9. A series of images in which a flow of 0.025 ml/min is produced, using the syringe pump, along the main channel (moving rightward). The fluid in the side arm is vibrated at different amplitudes in each image, with the images taken once transient effects have largely subsided, the vibration amplitudes are 45, 48, 53, 60,75, and 100 μm from (a) to (f) respectively. The distance across the channel over which mixing occurs between the two fluids is clearly increased with raised amplitude, and at the upper three amplitudes extends across the full width.
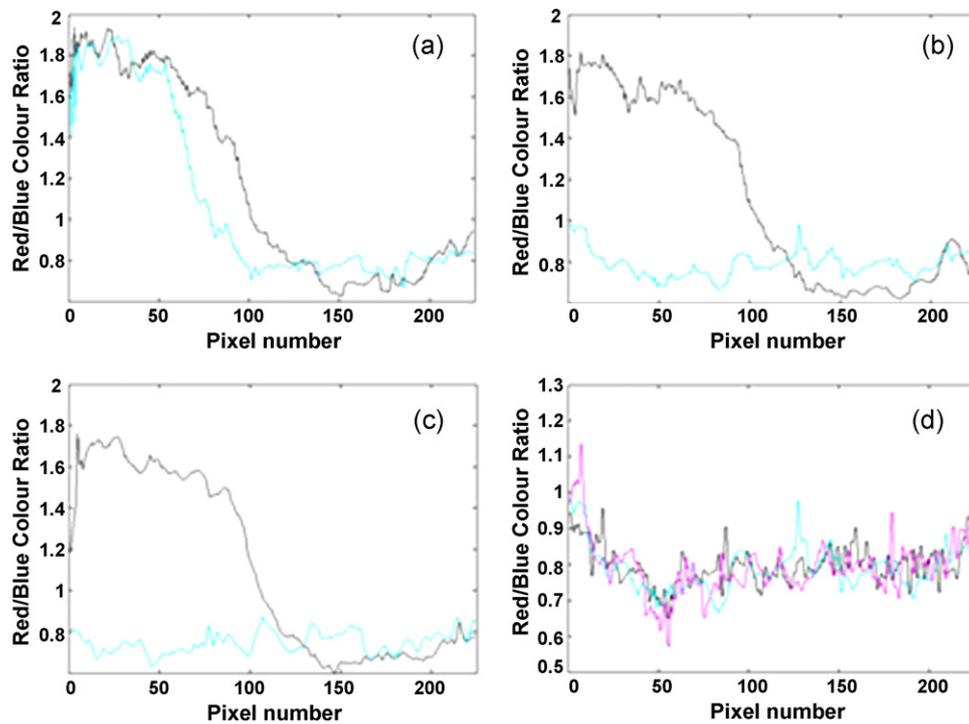
Fig. 10. A series of graphs depicting the colour intensity across the main channel width. The intensity is shown as a ratio between red and blue in the image taken. For (a–c) the black line depicts the ratio prior to activation of the side channel, whilst the cyan line is afterwards, in both cases the line examined is the data is taken by averaging the readings from the 20 most rightward (vertical) lines in the image. The cyan lines relate to excitation of 45, 60 and 100 μm for (a–c) respectively. Graph (d) shows data after excitation at 60 μm amplitude for three different bands of lines, again an average is taken over 20 lines, the cyan line is for the most rightward set of lines, the black and magenta are for sets of image lines offset by 25 and 50 pixels leftward, respectively. (For interpretation of the references to color in this figure legend, the reader is referred to the web version of the article.)

through the junction. Fig. 3 plots data acquired over a single oscillation cycle (1/100th of a second), for a case in which the oscillation is applied without a through-flow in the main channel. Fig. 3a shows streaklines traced by streams of particles injected from two points located at the intersection of the side arm and main channel (i.e. on the line $y = -1$ in Fig. 3a). Due to reflective symmetry in the flow, only injection points on the left half of the model are shown. The velocity component perpendicular to the main channel at the injection points over the oscillation cycle is shown in Fig. 3b, which demonstrates that over approximately the first half of the simulation, particles streams will move into the main channel from their injection points, before being carried towards the side channel by the reversing flow over the second half of the cycle. Comparing points A and B, the markedly different streakline patterns in Fig. 3a occur as a result of the different phase and amplitude of the velocity at the injection points (ref. Fig. 3b).

The proposed mixing mechanism requires that during the inflow phase, fluid enter the main channel from the side arm approximately perpendicular to the main channel, whereas in the outflow phase, fluid re-enter the side arm in a sink-like fashion, with velocity vectors at the junction with the side arm adopting larger angles from the side-arm centreline with distance from the centerline. In Fig. 3c, the magnitudes of the angles from the side-arm centreline of velocity at points A and B are plotted over the oscillation cycle. This data verifies that at these points the velocity vectors during the inflow phase are nearer to perpendicular to the main channel than during the return phase. During the inflow phase, the average inclination angle from the perpendicular at points A and B is approximately 12° and 3°, respectively, whereas during the outflow phase, angles of approximately 23° and 7° were computed.

Two crucial points underpinning this mixing mechanism may be noted from Fig. 3. Firstly, flow reversibility (or symmetry) between the inflow and outflow phases of the oscillation cycle has been bro-

ken. This is evidenced by the streakline patterns not terminating at the original injection point, nor retracing their outward paths on their return journeys. Secondly, evidence of the invocation of a region of circulating flow is shown by the positions of the oldest particles relative to the most recently injected particles. At point A, the oldest particles are displaced some 100 μm into the side arm after one oscillation period, whereas at point B, the oldest particles have migrated approximately 80 μm into the main channel. Therefore, the fluid near the centerline of the side arm experiences a net displacement towards the main channel every cycle, whereas the fluid nearer the side arm wall experiences a net displacement away from the main channel.

The net movement of fluid suggested by the data from a single oscillation cycle in Fig. 3 is demonstrated in Fig. 4 to be part of a longer-timescale circulation of fluid in the vicinity of the junction. The streakline patterns in Fig. 4 are computed over 20 oscillation cycles. The plots show that at the intersection of the main channel and side arm, a large recirculation is generated by the imposition of the sinusoidal oscillation in the side arm. On the left half of the geometry, this circulation is anticlockwise, and this is matched by a reflectively symmetric clockwise circulation on the right-hand half of the junction. The streakline patterns clearly show that fluid is progressively transported by this mixing mechanism from near the side-arm centerline into the main channel to a distance approximately twice the width of the side arm, before moving back towards the side-arm centerline near the main channel wall. It can be seen by the different proportion of a complete cycle traced by the particles in Fig. 4 that the time for a parcel of fluid to return to its original position is dependent on its starting position. This means that fluid parcels will be progressively dispersed relative to each other from one oscillation cycle to the next, indicating that the fluid is undergoing mixing. Importantly, the plot on the right of Fig. 4 demonstrates that this circulation penetrates into the side arm. Therefore fluid

from within the side arm is mixed with fluid in the main channel in this regime even when no net flow is imposed in the main channel.

The numerical model shows that swirling patterns can be obtained by simple oscillation of the fluid in a single channel, rather than vibration of the whole chip. Hence the erstwhile experimental set method [20] can be altered accordingly. A fluid filled pipe was attached to the sidearm, and this fluid was oscillated by attaching the plunger of the syringe at the end of the pipe to the shaker unit. Note that due to the reversibility of the actuation method, there is no net flow out of the side arm. Furthermore, there is no flow of fluid along the main channel. This set-up is depicted in Fig. 1, in all of the following experiments (except Fig. 8) the shaker is used, the speaker having been removed from the set-up. When the system is filled with a fluid based copolymer particle suspension (15 μm diameter beads, Bangs Laboratories Inc., with a concentration of approximately 5% solids in water) and actuated at 100 Hz, a counter clockwise swirl is seen on the left of the exit, and clockwise on the right (Fig. 5); which is consistent with expectations. The apparent stretching of the particle path due to the long exposure time compared to the oscillation frequency, allows calibration of the degree of fluid pulsing. Here, the amplitude of vibration was approximately 65 μm. A red dot has been added to the images to trace some particles through the rotation, which lasts about one fifth of a second. This was clearly unsynchronised in time with the alternating drive signal. The furthest distance reached by this swirl was 400 μm across the main channel width. Clearly the swirling pattern on the right-hand side of the exit is the stronger of the two; which is likely due to a slight drift of fluid along the channel as the flow was unregulated.

Whilst the swirling clearly exists it is worth noting that particles following this trajectory also have a superimposed vibrational movement due to the oscillation. This can be seen in Fig. 6, for two different amplitudes of vibration, 45 and 60 μm amplitude in the side arm. In these still images, a clear patch of fluid is seen at either side of the side arm exit, characteristic of swirling taking place. However it can also be seen that particle paths along the outer circumference of this region appear elongated (hence are vibrating faster than the camera shutter speed). The furthermost extent at which this occurs is clearly different for the two cases, with the lower oscillation causing vibration up to a distance of 260 μm away from the side arm exit, whilst for the higher amplitude case this distance increases to 550 μm. At the lower excitation amplitude, this vibrational effect causes a significant oscillation even within the jetting area of the swirl.

A combination of numerical simulation and physical experiments has demonstrated the swirl mixing mechanism without a through-flow. Hereafter, further experiments investigate the generalized case featuring a through-flow. In the usual side-by-side laminar flow of two fluids along a channel, only diffusion acting as a mixing mechanism, however, mixing can be rapidly hastened by such swirling. In order to demonstrate this, blue and red dyed water was introduced via the two arms entering the main channel, whilst the side arm was filled with blue fluid. The dyes used are standard food dyes, the colour intensities are normalized when image analysis is performed. When no net flow occurs in the main channel, and a vibration of amplitude 45 μm is produced in the side arm, a plume shaped feature is produced in the main channel. This happens as blue fluid jets out and draws in red fluid around the outside of the swirling patterns. This can be seen from the series of images presented in Fig. 7. The extent that this plume reaches across the main channel is evident; and increases to nearly reaching the far wall. The effect is clearly well localised at the exit of the side arm.

This localised plume effect can be well contrasted with what occurs when the whole chip is vertically vibrated. Fig. 8 shows the result of such an experiment, where the main channel has blue and red fluid, the side arm fluid in red, and there is a net flow in the main

channel of 0.01 ml/min moving leftwards. After 0.08 s of vibration, mixing of the fluids is clearly seen at the junction of the side arm and main channel as well. This is carried along the channel by the net flow wherein the mixing region appears to travel rightwards as well; indicating the result of mixing also occurring at the entrance to the main junction (i.e. the location at which the red and blue fluids first meet). So whilst mixing is well demonstrated, the location is not defined, as it could in effect occur at any junction.

Fig. 9 demonstrates mixing of flowing fluids under excitation by vibration of the side arm. This mixing is well localised at the side arm exit. The images show the fluid after the transient effects have died down, in each case the flow rate along the main channel is 0.025 ml/min. The parameter varied is the vibrational amplitude in the side arm. It can be seen that for low amplitudes the plume, a narrow mixed area is engendered extending a little more than half way across the channel. However, at higher amplitudes a full mix is easily achieved. The effect of the mixing has been analysed by pixel analysis of the images as depicted in Fig. 10. The images are recorded in reflective lighting. The ratio of red and blue image intensity has been analysed before and after actuation occurs. At 45 μm amplitude (consistent with Fig. 9a) only a small difference is observed in Fig. 10a, whilst at 60 μm (image Fig. 9d) the plot of the ratio of intensities in Fig. 10b is nearly flat across the channel width. At 100 μm amplitude (refer to image Fig. 9f) this line, shown in Fig. 10c, does become flat. An analysis of the ratio at different lengths along the channel is shown in Fig. 10d. The uniformity of the shapes of these lines demonstrates that the mixing has occurred over a very short spatial length.

The method described here contrasts sharply with the opposing side channel architecture [4,5] in that it offers asymmetry between fluid entering and leaving the side channels to create strong swirling. The use of only one side channel also ensures that liquid is drawn in upstream and to some extent downstream of the main flow to participate in mixing during each cycle. The ability to mix effectively in such a manner lends to potential useful applications such as the blending of reagents in capillary well microplates [30]; an approach that promises to enhance high throughput screening with small liquid volumes.

4. Conclusions

We have been able to account for here the predominant mechanism causing the swirling patterns at microfluidic junctions when perturbed mechanically at low frequencies [20]. Based on this, we show that harmonically vibrating the fluid in a side arm causes mixing to be established between two fluids moving through the main channel of the system. This method affords a highly localised mixing method, with minimal vibrational coupling to the rest of the system and as such lends itself well to microscopic investigation of the mixed fluid.

References

[1] A.D. Stroock, S.K.W. Dertinger, A. Adjari, I. Mezic, H.A. Stone, G.M. Whitesides, Chaotic mixer for microchannels, Science 295 (2002) 647–651.
[2] K. Malecha, L.J. Golonka, J. Baldyga, M. Jasinska, P. Sobieszuk, Serpentine microfluidic mixer made in LTCC, Sens. Actuators B 143 (2009) 400–413.
[3] Z. Lu, J. McMahon, H. Mohamed, D. Barnard, T.R. Shaikh, C.A. Mannella, T. Wagenknecht, T.M. Lu, Passive microfluidic device for sub millisecond chaotic mixing, Sens. Actuators B 144 (2010) 301–309.
[4] F. Okkels, P. Tabeling, Spatiotemporal resonances in mixing of open viscous fluids, Phys. Rev. Lett. 92 (2004) 038301.

[5] X. Niu, L. Liu, W. Wen, P. Sheng, Hybrid approach to high-frequency microfluidic mixing, Phys. Rev. Lett. 97 (2006) 044501.

[6] M.J. Kim, K.S. Breuer, Controlled mixing in microfluidic systems using bacterial chemotaxis, Anal. Chem. 79 (2007) 955–959.

[7] E. Biddiss, D. Erickson, D. Li, Charge enhanced micro-mixing for electrokinetic flows, Anal. Chem. 76 (2004) 3208–3213.

[8] T.J. Johnson, D. Ross, L.E. Locascio, Rapid microfluidic mixing, Anal. Chem. 74 (2001) 45–51.

[9] S.P. Martin, R.J. Townsend, L.A. Kuznetsova, K.A.J. Borthwick, M. Hill, M.B. McDonnell, W.T. Coakley, Spore and micro-particle capture on an immunosensor surface in an ultrasound standing wave system, Biosens. Bioelectron. 21 (2005) 758–767.

[10] A. Neild, S. Oberti, J. Dual, Design, modeling and characterization of microfluidic devices for ultrasonic manipulation, Sens. Actuators B 121 (2007) 452–461.

[11] A. Neild, S. Oberti, G. Radziwill, J. Dual, Simultaneous positioning of cells into two-dimensional arrays using ultrasound, Biotechnol. Bioeng. 97 (August (5)) (2007) 1335–1339.

[12] S. Oberti, A. Neild, J. Dual, Manipulation of micrometer sized particles within a micromachined fluidic device to form two-dimensional patterns using ultrasound, J. Acoust. Soc. Am. 121 (2007) 778–785.

[13] G.G. Yaralioglu, I.O. Wygant, T.C. Marentis, B.T. Khuri-Yakub, Ultrasonic mixing in microfluidic channels using integrated transducers, Anal. Chem. 76 (2004) 3694–3698.

[14] K. Sritharan, C.J. Strobl, M.F. Schneider, A. Wixforth, Z. Guttenberg, Acoustic mixing at low Reynold's numbers, Appl. Phys. Lett. 88 (2006) 054102.

[15] C.J. Strobl, Z. von Guttendegr, A. Wixworth, Nano- and pico-dispensing of fluids on planar substrates using SAW, IEEE Trans. Ultrason. Ferroelectr. Freq. Control 51 (2004) 1432–1436.

[16] A.J. Slobodnik, Surface acoustic waves and SAW materials, Proc. IEEE 64 (1976) 581–595.

[17] A.S. Ergun, Y. Huang, X. Zhuang, O. Oralkan, G.G. Yarahoglu, B.T. Khuri-Yakub, Capacitive micromachined ultrasonic transducers: fabrication technology, IEEE Trans. Ultrason. Ferroelectr. Freq. Control 52 (2005) 2242–2258.

[18] P. Brunet, J. Eggers, R.D. Deegan, Vibration-induced climbing of drops, Phys. Rev. Lett. 99 (2007) 144501.

[19] J. Whitehill, A. Neild, T.W. Ng, M. Stokes, Collection of suspended particles in a drop using low frequency vibration, Appl. Phys. Lett. 96 (2010) 053501.

[20] S. Oberti, A. Neild, T.W. Ng, Microfluidic mixing under low frequency vibration, Lab Chip 9 (2009) 1435–1438.

[21] S.H. Wong, M.C.L. Ward, C.W. Wharton, Micro T-mixer as a rapid mixing micromixer, Sens. Actuators B 100 (2004) 359–379.

[22] S.B. Müller, L. Kleiser, Viscous and inviscid spatial stability analysis of compressible swirling mixing layers, Phys. Fluids 20 (2008) 114103.

[23] Y. Ito, S. Komori, A vibration technique for promoting liquid mixing and reaction in a microchannel, AIChE J. 52 (2006) 3011–3017.

[24] I. Glasgow, N. Aubry, Enhancement of microfluidic mixing using time pulsing, Lab Chip 3 (2003) 114–120.

[25] F. Bottausci, C. Cardonne, C. Meinhart, I. Mezic, An ultrashort mixing length micromixer: the shear superposition micromixer, Lab Chip 7 (2007) 396–398.

[26] G.J. Sheard, T. Leweke, M.C. Thompson, K. Hourigan, Flow around an impulsively arrested circular cylinder, Phys. Fluids 19 (2007) 083601.

[27] G.J. Sheard, M.J. Fitzgerald, K. Ryan, Cylinders with square cross section: wake instabilities with incidence angle variation, J. Fluid Mech. 630 (2009) 43–69.

[28] G. Coppola, S.J. Sherwin, J. Pieró, Non-linear particle tracking for high-order elements, J. Comput. Phys. 172 (2001) 356–386.

[29] R.J. Dijkink, J.P. van der Dennen, C.D. Ohl, A. Prosperetti, The acoustic scallop: a bubble-powered actuator, J. Micromech. Microeng. 16 (2006) 1653–1659.

[30] T.W. Ng, Y. Yu, H.Y. Tan, A. Neild, Capillary wells microplate, Appl. Phys. Lett. 93 (2008) 174105.

Biographies

Adrian Neild received a PhD in engineering from the University of Warwick, in 2003. Subsequently, he worked as a postdoctoral researcher at the Institute for Mechanical Systems at ETH Zurich (Swiss Federal Institute of Technology Zurich). He has been a faculty member at Monash University since 2006, his research interests are in the fields of ultrasound, the use of acoustics for actuation of microfluidic systems and particle manipulation.

Tuck Wah Ng's research interests are in instrumentation (particularly optical) development, particle/cell manipulation, and biochemical analysis techniques. He is member of the Optical Society of America and SPIE. He has published over 100 journal articles and recepient of the Valued Reviewer Award 2009 from Sensors and Actuators A.

Gregory J. Sheard received his B.E. (Hons) in Mechanical Engineering in 2000 and his Ph.D. specialising in wake dynamics and stability in 2004 from Monash University, Melbourne, Australia. He subsequently undertook a postdoctoral fellowship developing computational fluid dynamics algorithms for the study of biological fluid flows in collaboration with the School of Physiology at Monash University from 2005. He is presently employed as a Senior Lecturer in the Faculty of Engineering, Monash University, where he specialises in the development and application of high-order computational fluid dynamics algorithms with applications spanning capillary flows through to planetary atmospheric dynamics, and has published over 40 papers in both journals and proceedings of international conferences.

Matthew Powers received his Bachelors Degree from the Department of Mechanical and Aerospace Engineering at Monash University in 2009. His final year project work was on using acoustics to induce mixing in microfluidic systems.

Stefano Oberti got his degree in mechanical engineering from the Swiss Federal Institute of Technology in 2004. During his studies he specialized in micro and nanotechnology as well as control systems. After completion of his diploma thesis at the IBM Zurich Research Laboratory on distance measurements in liquid environment based on the force generated by the fluid squeezed between two surfaces, he entered the field of acoustic particle manipulation. Until 2009, when he got his PhD from the Swiss Federal Institute of Technology, he investigated manipulation of suspended micron sized particles by means of acoustic fields within micromachined fluidic systems.